Title

Choanoflagellate transfection illuminates their cell biology and the ancestry of animal septins

Short Title

Robust transfection in choanoflagellates

Authors

David S. Booth[1], Heather Szmidt-Middleton, and Nicole King[2]*

Howard Hughes Medical Institute and Department of Molecular and Cell Biology
University of California, Berkeley
Berkeley, CA 94720

[1] https://orcid.org/0000-0002-4724-4702
[2] https://orcid.org/0000-0002-6409-1111

*Corresponding author
Email: nking@berkeley.edu
Phone: (510) 643-9395

ABSTRACT

As the closest living relatives of animals, choanoflagellates offer unique insights into animal origins and core mechanisms underlying animal cell biology. However, unlike traditional model organisms, such as yeast, flies and worms, choanoflagellates have been refractory to DNA delivery methods for expressing foreign genes. Here we report the establishment of a robust method for expressing transgenes in the choanoflagellate *Salpingoeca rosetta*, overcoming barriers that have previously hampered DNA delivery and expression. To demonstrate how this method accelerates the study of *S. rosetta* cell biology, we engineered a panel of fluorescent protein markers that illuminate key features of choanoflagellate cells. We then investigated the localization of choanoflagellate septins, a family of GTP-binding cytoskeletal proteins that are hypothesized to regulate the multicellular rosette development in *S. rosetta.* Fluorescently tagged septins localized to the basal pole of *S. rosetta* single cells and rosettes in a pattern resembling septin localization in animal epithelia. The establishment of transfection in *S. rosetta* and its application to the study of septins represent critical advances in the growth of *S. rosetta* as an experimental model for investigating choanoflagellate cell biology, core mechanisms underlying animal cell biology, and the origin of animals.

38 **INTRODUCTION**

39 First described in the mid-19th century, choanoflagellates inspired great debate regarding
40 animal taxonomy (James-Clark, 1868; Kent, 1871; Leadbeater, 2015). The most diagnostic
41 morphological feature of choanoflagellates, a "collar complex" composed of a single apical
42 flagellum surrounded by a collar of actin-filled microvilli (Fig. 1), was interpreted as evidence of
43 a special relationship between choanoflagellates and sponges, whose choanocytes (or "collar
44 cells") each bear a collar complex. Subsequent phylogenetic analyses and the discovery of cells
45 with a collar complex in nearly all animal phyla have revealed that sponges and all other
46 animals are monophyletic, with choanoflagellates as their closest living relatives (Fig. 1) (Lang
47 *et al.*, 2002; King *et al.*, 2008; Ruiz-Trillo *et al.*, 2008; Burger *et al.*, 2003; Fairclough *et al.*, 2013;
48 Brunet and King, 2017). Moreover, comparative genomic analyses have revealed that
49 choanoflagellates, animals, and other holozoans express genes required for animal
50 multicellularity and embryogenesis (Richter *et al.*, 2018; Sebe-Pedros *et al.*, 2017), including
51 cadherins (Abedin and King, 2008), tyrosine kinases (Suga *et al.*, 2012; Manning *et al.*, 2008),
52 and Myc (Young *et al.*, 2011). Thus, comparisons among animals and choanoflagellates have
53 the potential to provide unique insights into animal origins and core features of animal cell
54 biology that are not conserved in other experimental models, such as yeast (King, 2004).

55 The choanoflagellate *Salpingoeca rosetta* (previously named *Proterospongia* sp. (King *et*
56 *al.*, 2003)) has recently emerged as an experimentally tractable model. *S. rosetta* develops from
57 a single founding cell into a spherical, multicellular "rosette" (Fig. 1C) through serial rounds of
58 cell division in a process that evokes the earliest stages of animal embryogenesis (Fairclough *et*
59 *al.*, 2010). Since the establishment of the first *S. rosetta* cultures almost twenty years ago, *S.*
60 *rosetta* has become increasingly amenable to cell and molecular biological approaches due to
61 the sequencing of its genome (Fairclough *et al.*, 2013), the establishment of forward genetic
62 screens (Levin and King, 2013; Levin *et al.*, 2014), the ability to experimentally control key
63 events in its life history (Dayel *et al.*, 2011), and the discovery that environmental bacteria
64 induce multicellular rosette development and mating (Alegado *et al.*, 2012; Dayel *et al.*, 2011;
65 Woznica *et al.*, 2016; Woznica *et al.*, 2017).

66 An important remaining barrier to the study of molecular and cellular mechanisms in *S.*
67 *rosetta* has been the inability to perform transfection and transgene expression. Furthermore,
68 the absence of the RNA interference pathway in *S. rosetta* has precluded gene knockdowns
69 (Richter *et al.*, 2018; Fairclough *et al.*, 2013). Here we report the establishment of a robust

70 nucleofection-based method to transfect and express transgenes in *S. rosetta.* By engineering
71 plasmids with *S. rosetta* regulatory sequences driving the expression of fluorescently-tagged *S.*
72 *rosetta* proteins, we have developed a broad panel of markers for the study of choanoflagellate
73 cell biology *in vivo*. As a first application, we used transgene expression to characterize septins,
74 genes with conserved roles in fungal (Helfer and Gladfelter, 2006; Berepiki and Read, 2013)
75 and animal development (Fairclough *et al.*, 2013; Adam *et al.*, 2000; Neufeld and Rubin, 1994;
76 O'Neill and Clark, 2013; Kim, S. K. *et al.*, 2010), that have been hypothesized to regulate rosette
77 development (Fairclough *et al.*, 2013). By imaging fluorescently-tagged septins in live cells, we
78 show that their localization in *S. rosetta* resembles that in animal epithelia, providing a potential
79 evolutionary link between the mechanisms underlying animal and choanoflagellate
80 multicellularity.
81

82 **RESULTS**

83 **A robust method to transfect *S. rosetta***

84 To detect successful transfection, we started by engineering four different DNA plasmid
85 constructs, each with different *S. rosetta* regulatory sequences fused to a gene, *nanoluc* (Hall *et*
86 *al.*, 2012), encoding a highly sensitive luciferase (Fig. S1B). Because no choanoflagellate
87 promoters had previously been mapped, we increased the likelihood of cloning sequences that
88 would drive robust gene expression by fusing *nanoluc* to non-coding sequences flanking a set of
89 genes – *elongation factor L (efl)*, *α-tubulin (tub)*, *non-muscle actin (act)*, and *histone H3 (H3)* –
90 that each exhibit high expression, lack introns in their open reading frames and have well-
91 annotated 5'- and 3'-untranslated regions (Fig. S1A) (Fairclough *et al.*, 2013).
92 Next, we set out to deliver these DNA plasmid constructs into *S. rosetta* cells using
93 nucleofection, an electroporation-based technique that has proven particularly effective for
94 transfection of diverse eukaryotes (Janse, Ramesar *et al.*, 2006; Caro *et al.*, 2012; Vinayak *et*
95 *al.*, 2015), including mammalian primary cells that are resistant to transfection (Gresch *et al.*,
96 2004; Hamm *et al.*, 2002). To quantify transfection efficiency, we performed luciferase assays
97 on cell lysates. Through many trials, we eventually achieved a low level of transfection with
98 nucleofection by improving conditions for culturing *S. rosetta* cells (Fig. S2), modifying
99 approaches for handling cells throughout the nucleofection procedure (Supplementary
100 Information), and screening thirty unique combinations of electrical pulses and buffers (Fig. S3).

101 Optimization around these initial conditions culminated in a procedure that provided robust
102 and reproducible transfection of *S. rosetta* (Fig. 2A; Methods and
103 http://www.protocols.io/groups/king-lab). When used in the optimized transfection procedure, all
104 four transfection reporters drove strong expression of nanoluc protein, producing luminescence
105 signals that were over three orders of magnitude above the detection limit (Fig. 2B).
106 Because this was the first example, to our knowledge, of successful transgene expression
107 in any choanoflagellate, we sought to identify which steps in the optimized protocol were most
108 essential. Using the p*H3-nanoluc* transfection reporter, we quantified how the omission of each
109 step impacted transfection efficiency (Fig. 2C). In addition to the use of an optimal electrical
110 pulse during nucleofection, the two most important steps were priming the cells through the
111 enzymatic removal of the extracellular matrix prior to nucleofection (Fig. 2A, step 1; Fig. S4) and
112 the inclusion of carrier DNA during nucleofection (Fig. 2A, step 2; Fig. S5); eliminating either of
113 these steps resulted in a nearly complete loss of signal.
114 Priming the cells for nucleofection was a novel step motivated by our observation that *S.*
115 *rosetta* cells are surrounded by a potentially protective extracellular coat (Dayel *et al.*, 2011;
116 Levin *et al.*, 2014; Leadbeater, 2015), and the inclusion of carrier DNA (pUC19) in nucleofection
117 reactions eliminated the need to include large quantities of reporter construct plasmid (Fig. S5).
118 Another improvement was the development of a recovery buffer that enhanced transfection ten-
119 fold (Fig. 2A, step3), presumably by promoting membrane resealing after nucleofection (Rols
120 and Teissie, 1990; Rols and Teissie, 1989).
121 Luciferase assays performed on cell lysates gave a sensitive read-out of population-wide
122 nanoluc expression but did not allow the examination of live, transfected cells nor reveal the
123 proportion of cells that were successfully transfected. Therefore, we next engineered eight
124 reporters with different fluorescent proteins placed under the control of regulatory sequences
125 from the *S. rosetta actin* homolog. Fluorescence was readily detected from cells transfected with
126 reporters encoding mTFP1 (Ai *et al.*, 2006), mWasabi (Ai *et al.*, 2008), sfGFP (Pedelacq *et al.*,
127 2006), mNeonGreen (Shaner *et al.*, 2013), mPapaya (Hoi *et al.*, 2013), TagRFP-T(Shaner *et al.*,
128 2008), mCherry (Shaner *et al.*, 2004), and tdTomato (Shaner *et al.*, 2004). In contrast, an eGFP
129 (Yang *et al.*, 1996) reporter failed to yield fluorescent cells, likely due to protein misfolding, as
130 cells transfected with the 'super-folder' variant of GFP (sfGFP) did fluoresce properly. In
131 transfected cells, the fluorescent signal was distributed throughout the nucleus and cytosol yet
132 excluded from membrane bound compartments (Fig. 3A).

133 We observed that transfected cells resembled untransfected cells in their shape, motility,
134 and ability to propagate, indicating that transfection did not irreparably harm *S. rosetta*.
135 Fluorescence persisted through multiple cell divisions, yet the diminishing signal in daughter
136 cells indicated that transfection was transient (Fig. S6A). Importantly, using flow cytometry one
137 to two days after transfection, we found that ~1% of the population was reproducibly
138 transfected, and fluorescence-activated cell sorting enriched this transfected cell population
139 (Fig. S6B). This transfection frequency is comparable to high frequency episomal transformation
140 of the model yeast *Saccharomyces cerevisiae* that ranges from 1 – 10% (Schiestl and Gietz,
141 1989; Kawai *et al.*, 2010), and similar transfection frequencies are achieved in model
142 apicocomplexans (Janse, Franke-Fayard *et al.*, 2006; Caro *et al.*, 2012).
143
144 **Fluorescent markers illuminate the cell architecture of *S. rosetta***
145 To demonstrate the versatility of the new method for transfection and simultaneously
146 explore the cell biology of *S. rosetta in vivo*, we designed a set of fluorescent reporters to mark
147 key features of *S. rosetta* cells: the nucleus, cytoplasm, collar, filopodia, flagellum, membrane,
148 mitochondria and endoplasmic reticulum (ER). For each fluorescent reporter, the *mCherry* gene
149 was fused in-frame to *S. rosetta* DNA sequences encoding conserved proteins or peptides that
150 localize to specific organelles or subcellular regions in yeast and mammalian cells. To
151 benchmark each fluorescent marker, we compared its localization in transfected cells to cellular
152 landmarks known from electron and immunofluorescence micrographs (Fig. S7) (Abedin and
153 King, 2008; King *et al.*, 2009; King *et al.*, 2008; Sebe-Pedros *et al.*, 2013; Leadbeater, 2015).
154 Electron micrographs have revealed two distinct regions in the nucleus: the darkly-stained
155 nucleolus positioned in the center and the surrounding, more lightly-stained nucleoplasm
156 (Leadbeater, 2015; Burkhardt *et al.*, 2014). As predicted, mCherry fused to either the carboxy
157 terminus of H3 or the amino terminus of the simian virus 40 nuclear localization signal localized
158 primarily to the *S. rosetta* nucleoplasm and was excluded from the cytoplasm (Fig. 3B, C)
159 (Kanda *et al.*, 1998; Kalderon *et al.*, 1984). In contrast, the cytoplasmic marker EFL-mCherry
160 (Huh *et al.*, 2003) localized to the cytosol and was excluded from the nucleus (Fig. 3D).
161 Two of the most diagnostic features of the choanoflagellate cell are the actin-filled collar
162 and the flagellum, which is comprised of microtubules (Karpov and Leadbeater, 1998). A fusion
163 of mCherry to the filamentous actin-binding peptide Lifeact (Riedl *et al.*, 2008) highlighted the
164 parallel arrangement of straight microvilli in the collar (Fig. 3G and 3J), as well as filopodia
165 extending from the basal pole of the cell (Fig. 3G, lower arrow)(Karpov and Leadbeater, 1998;

166 Sebe-Pedros *et al.*, 2013). In live cells, Lifeact-mCherry revealed the native structure of the
167 collar, which can be distorted in cells fixed for staining with fluorescent phalloidin or actin
168 antibodies (Sebe-Pedros *et al.*, 2013). Lifeact-mCherry also showed details of actin filament
169 organization that have not previously been evident, such as the existence of actin filaments that
170 originate in the cell body and coalesce at the base of the collar to form each microvillus (Fig.
171 3G', upper arrow; improved immunofluorescence techniques also preserve these cortical actin
172 filaments, Fig. 1B). A fusion of α-tubulin to mCherry (Straight *et al.*, 1997) illuminated individual
173 cortical microtubules emanating from the base of the flagellum to the basal pole of the cell (Fig.
174 3K', arrow) and allowed visualization of the rapidly beating flagellum in live cells (Fig. 3H and
175 3K).
176 A cell membrane marker, with a geranyl-geranylation sequence fused to mCherry (Wang
177 and Casey, 2016; Reid *et al.*, 2004), outlined the entire cell, including the flagellum, collar, and
178 cell body (Fig. 3I and 3L), and faintly marked the Golgi apparatus (Fig. 3I', arrow). In live cells,
179 the cell membrane marker captured the formation of a phagocytic cup engulfing bacterial prey
180 (Fig. S8)(Dayel and King, 2014). The ER marker (Friedman *et al.*, 2011), which included the
181 amino terminal signal sequence from the secreted protein Rosetteless (Levin *et al.*, 2014) and a
182 carboxy terminal ER retention sequence from the ER resident chaperone BiP (PTSG_07223),
183 highlighted the continuity of the ER with the nuclear envelope and the distribution of ER
184 throughout the cell, including around vacuoles (Fig. 3F). A mitochondrial marker (Friedman *et*
185 *al.*, 2011) with an amino terminal targeting sequence from *S. cerevisiae* Cytochrome C Oxidase,
186 Subunit IV revealed a network of mitochondria (Nunnari *et al.*, 1997) that is enriched around the
187 nucleus and extends throughout the cell (Fig. 3G). Taken together, these fluorescent markers
188 demonstrate new experimental capabilities to rapidly tag proteins and to monitor their
189 localization in distinct cellular compartments and locales.
190
191 **Transgenesis reveals septin localization in live *S. rosetta* single cells and rosettes**
192 A major motivation for establishing transgenics in *S. rosetta* was to rapidly characterize
193 candidate genes for multicellularity. Therefore, we investigated the localization of septins, a
194 family of paralogous genes hypothesized to contribute to multicellular development in *S. rosetta*
195 (Fairclough *et al.*, 2013). The assembly of septin monomers into higher order structures is
196 important for septin localization (McMurray *et al.*, 2011) and for the conserved roles of septins in
197 regulating cytokinesis and cell polarity in fungi and animals. In animals, septins also function in
198 phagocytosis (Huang *et al.*, 2008), ciliogenesis (Hu *et al.*, 2010), and planar cell polarity (Kim *et*

199 *al.*, 2010). Septin proteins have a characteristic domain architecture with a diagnostic amino
200 terminal guanosine triphosphate binding domain (G-domain), and most septins also have a
201 carboxy terminal coiled-coil domain (Pan *et al.*, 2007; Nishihama *et al.*, 2011) (Fig. 4A). Septin
202 paralogs interact directly through their G-domains to form heteromeric filaments, and these
203 heteromeric filaments interact with each other through the septin coiled-coil domains to form
204 higher order assemblies (Bertin *et al.*, 2008; Garcia *et al.*, 2011; Sirajuddin *et al.*, 2007).
205 *S. rosetta* expresses four septin paralogs, three of which have well-annotated genome
206 models in the current draft genome (Fairclough *et al.*, 2013). We started by examining the
207 localization of the *S. rosetta* septin protein *Sr*Septin2 (PTSG_07215), a septin with domains
208 conserved in human and fungal septins (Fairclough *et al.*, 2013) that are necessary for septin
209 filament formation (Sirajuddin *et al.*, 2007; Bertin *et al.*, 2008). Strikingly, mTFP1-*Sr*Septin2 was
210 enriched at the basal poles of single and rosettes cells (Fig. 4B and 4E) and at points of contact
211 between adjacent cells in rosettes (Fig. 4E). This mTFP1-*Sr*Septin2 fusion likely revealed the
212 native localization of *Sr*Septin2 in *S. rosetta* because septins visualized by immunofluorescence
213 microscopy in yeast (Ford and Pringle, 1991; Kim, H. B. *et al.*, 1991; Cid *et al.*, 1998; Haarer
214 and Pringle, 1987), *Drosophila* (Adam *et al.*, 2000; Silverman-Gavrila *et al.*, 2008; Neufeld and
215 Rubin, 1994), and mammalian cells (Spiliotis *et al.*, 2008) display the same localization as
216 septins tagged with fluorescent proteins.
217 To investigate whether *Sr*Septin2 localized to the basal pole of cells might be part of
218 heteromeric septin filaments, we examined the localization of another septin paralog, *Sr*Septin6
219 (PTSG_06009) and found that *Sr*Septin6 displays the same basal localization as *Sr*Septin2 (Fig.
220 4C). Such colocalization (Fig. S9) and the sequence homology with septins that have previously
221 been shown to form heteromeric filaments (Sirajuddin *et al.*, 2007) strongly suggests that
222 *Sr*Septin2 and *Sr*Septin6 assemble together at the basal pole. We further found that the basal
223 localization of *Sr*Septin2 requires the coiled-coil domain, as a complete deletion of the coiled-
224 coil domain (SrSeptin2ΔCC; Fig. 4A, D, F) eliminated *Sr*Septin2 enrichment at the basal pole
225 when expressed in wild-type cells. Unexpectedly, mTFP1-*Sr*Septin2ΔCC formed ectopic rings
226 around vesicles in the cytosol in wild-type cells (Fig. 4D and 4F). The localization of mTFP1-
227 *Sr*Septin2ΔCC resembled the formation of ectopic septin filaments at convex membranes and
228 the depletion of septins at the concave membranes in the filamentous fungi *Ashbya gosypii*
229 (Meseroll *et al.*, 2012) upon the deletion of the coiled-coil domain of the fungal septin Shs1p.
230 Similarly, vesicles to which mTFP1-*Sr*Septin2ΔCC localized have convex membranes as

231 opposed to the concave membrane at the basal end of *S. rosetta* where wild-type *Sr*Septin2
232 localized.
233 The basal and lateral localization of *Sr*Septin2 and *Sr*Septin6 in rosettes is reminiscent of
234 septin localization in polarized epithelial cells (Fares *et al.*, 1995; Spiliotis *et al.*, 2008), in which
235 septins interact with the positive ends of microtubules that are growing toward the basal pole
236 (Bowen *et al.*, 2011). In choanoflagellates, microtubules radiate down from the apical
237 microtubule organizing centers (Karpov and Leadbeater, 1998), with the plus ends meeting at
238 the basal pole of each cell, similar to the orientation of microtubule plus ends toward the basal
239 pole in animal epithelia (Meads and Schroer, 1995). To examine if septins also interact with the
240 plus ends of microtubules in *S. rosetta*, we co-transfected cells with mTFP1-*Sr*Septin2 and the
241 tubulin marker α-tubulin-mCherry (Fig. 4G). Fluorescence microscopy showed that septin
242 filaments intercalate between cortical microtubules at the basal pole of the cell (Fig. 4G). These
243 data are consistent with conserved interactions between septins and microtubules from yeast to
244 animals (Kusch *et al.*, 2002; Kremer *et al.*, 2005; Sellin *et al.*, 2011; Spiliotis *et al.*, 2008),
245 including at the plus-ends of microtubules in choanoflagellates and animal epithelia (Bowen *et*
246 *al.*, 2011).
247

248 **DISCUSSION**

249 By synthesizing our growing knowledge of *S. rosetta* biology with a rigorous
250 characterization and optimization of each step in the transfection procedure, we have developed
251 a robust method for transgenesis in *S. rosetta* that can be easily implemented by other
252 laboratories. This method overcomes numerous barriers that prevented efficient DNA delivery in
253 our prior attempts using diverse methods, including standard electroporation, lipofection,
254 bombardment, and cell-penetrating peptides. A key breakthrough for this study was the
255 discovery that the extracellular coat surrounding *S. rosetta* might present a barrier for
256 transfection, which motivated the development of a method to gently remove the extracellular
257 material surrounding *S. rosetta,* thereby sensitizing cells for transfection. Additional
258 improvements to the transfection procedure, such as a step for promoting the closure of the
259 plasma membrane after electrical pulsation, were designed to address the unique challenges
260 that arise from culturing *S. rosetta* in sea water. Just as our method was informed by
261 approaches developed in model microeukaryotes (*Chlamydomonas* and yeast), the methods we
262 have established in *S. rosetta* will likely extend to aid gene delivery in diverse non-model marine

263 microeukaryotes. Overall, the gestalt of continually improving choanoflagellate husbandry (Levin
264 and King, 2013), developing protocols for priming and recovering cells during nucleofection, and
265 extensively optimizing transfection based on a quantitative assay produced a robust method for
266 gene delivery in *S. rosetta*.

267 This work also provides a foundational set of vectors for expressing transgenes in *S.*
268 *rosetta* (Dataset S1). In these vectors, the expression of luciferase or fluorescent proteins was
269 placed under the control of native regulatory elements. From these vectors, we constructed a
270 panel of fluorescently tagged subcellular markers that serve as references for monitoring the
271 localization of other proteins in *S. rosetta*. For example, through our pilot study of *Sr*Septin2 and
272 *Sr*Septin6, the use of these new transgenic tools revealed that septins localize to the basal pole
273 of choanoflagellates, mirroring their localization in animal epithelial cells (Spiliotis *et al.*, 2008;
274 Fares *et al.*, 1995).

275 Observing septin localization in *S. rosetta* contributes to our understanding of how septin
276 functions evolved prior to the evolution of an epithelium in stem animals. A hallmark of animal
277 epithelia is tightly connected cells that each have an apical and basal pole comprised of distinct
278 lipids, proteins, and cytoskeletal structures (Rodriguez-Boulan and Macara, 2014). Septins help
279 shape epithelia and other types of cells by serving as buttresses (Tanaka-Takiguchi *et al.*, 2009;
280 Tooley *et al.*, 2009) and diffusion barriers (Barral *et al.*, 2000; Takizawa *et al.*, 2000; Hu *et al.*,
281 2010) for membranes that have distinct geometries (Bridges *et al.*, 2016; Cannon *et al.*, 2018)
282 and lipid compositions (Casamayor and Snyder, 2003; Tanaka-Takiguchi *et al.*, 2009; Bertin *et*
283 *al.*, 2010; Bridges *et al.*, 2014) and by interacting with microtubules (Spiliotis, 2010) and
284 filamentous actin (Mavrakis *et al.*, 2014). While comparisons between animals and fungi have
285 revealed conserved functions of septins in cell organization (Spiliotis and Gladfelter, 2012), the
286 divergence of the lineages that gave rise to fungi and animals over one billion years ago
287 (Parfrey *et al.*, 2011) resulted in important differences in fungal and animal cell biology (Stajich
288 *et al.*, 2009). In fungi, septins facilitate polarized cell growth toward the new daughter cell (Kim
289 *et al.*, 1991; Berepiki and Read, 2013), compartmentalize connected daughter cells (Barral *et*
290 *al.*, 2000; Takizawa *et al.*, 2000; Helfer and Gladfelter, 2006) , and mediate cytokinesis
291 (Hartwell, 1971). In addition to their conserved roles in cell division (Neufeld and Rubin, 1994),
292 animal septins have specific functions in epithelia that maintain apical-basal polarity (Spiliotis *et*
293 *al.*, 2008), planar cell polarity (Kim *et al.*, 2010), intercellular adhesion (Kim, J. and Cooper,
294 2018; Park *et al.*, 2015) , and ciliogenesis (Hu *et al.*, 2010; Kim *et al.*, 2010). The basal
295 localization of septins in *S. rosetta* suggests that septin filaments organize a distinct region at

296 the basal end of the cell, perhaps supporting intercellular contacts at the basal ends of cells in
297 rosettes (Fig. 4E). Consistent with this hypothesis is the observation that the Rosetteless
298 protein, which is necessary for rosette development, localizes to the basal end of cells prior to
299 secretion into the interior of rosettes where the basal ends of cells meet (Levin *et al.*, 2014).
300 Continued study of septin function in *S. rosetta* will establish the mechanisms by which septins
301 facilitate multicellular development, and further comparisons with non-metazoan holozoans with
302 recently established transgenic methods, such as *Capsaspora owczarzaki* (Parra-Acero *et al.*,
303 2018) and *Creolimax fragrantissima* (Suga and Ruiz-Trillo, 2013), will provide further insights
304 into the ancestral functions of septins.
305 Previous analyses of gene function in choanoflagellates relied on custom antibodies
306 (Abedin and King, 2008; Young *et al.*, 2011; Burkhardt *et al.*, 2014; Levin *et al.*, 2014), laborious
307 forward genetic screens (Levin *et al.*, 2014), and *in vitro* biochemistry (Burkhardt *et al.*, 2014).
308 The ability to express transgenes in *S. rosetta* described here will accelerate studies of the
309 ancestral functions of animal genes that are conserved in choanoflagellates. We anticipate that
310 future work will build on this approach, eventually leading to the development of methods for
311 stable transgenesis and genome editing in *S. rosetta*. Combining an expanded repertoire of
312 approaches for investigating gene function in-depth in *S. rosetta* with comparisons to other
313 experimentally-tractable choanoflagellates (Li *et al.*, 2018; Richter *et al.*, 2018) and non-
314 choanozoans (Suga and Ruiz-Trillo, 2013; Parra-Acero *et al.*, 2018) promises to yield
315 increasingly mechanistic insights into the ancestry of animal cell biology.
316

317 ## MATERIALS AND METHODS

318

319 **Cell culture and media preparation**

320 *S. rosetta* was cultured with a single bacterial species, *E. pacifica*, that serves as a food
321 source (Levin and King, 2013). Media recipes are provided in Table S1. Cultures were
322 established from frozen aliquots by adding 1 ml of thawed cells to 10 ml of 0.2x High Nutrient
323 Media (Table S1). After the cells reached a density of 10^4 cells/ml, the culture was split 1:2 into
324 1x High Nutrient Media with a constant volume of 0.24 ml/cm^2. After this initial split (denoted as
325 day 0), cells were passaged in 1x High Nutrient Media according to the following schedule: 1:4
326 dilution on day 1, 1:8 dilution on day 2, 1:16 on day 3. Subsequently cells were passaged every
327 day at a 1:24 dilution or every other day as a 1:48 dilution of cells.

328 Based on the recommendation from Lonza to use a medium with a low calcium
329 concentration for transfecting mammalian cells, we searched for a seawater recipe with a lower
330 concentration of calcium than the routinely-used artificial seawater made from Tropic of Marin
331 Salts (Levin and King, 2013), which has a calcium concentration of 9.1 mM at a salinity of 35
332 g/kg (Atkinson and Bingman, 1998). The AK seawater formulation (Table S1) that has been
333 used to culture marine algae (Hallegraeff *et al.*, 2004) and dinoflagellates (Skelton *et al.*, 2009)
334 and has a calcium concentration of 2.7 mM. We found that *S. rosetta* grows more rapidly in 1x
335 High Nutrient Media prepared in AK seawater rather than seawater prepared with Tropic of
336 Marin Salts (Fig. S2A). Therefore, we switched to a growth medium based on AK seawater for
337 routine culturing. After optimizing the nucleofection protocol, we demonstrated that growing *S.*
338 *rosetta* in AK seawater also resulted in higher transfection efficiencies (Fig. S2B) than growing
339 *S. rosetta* in seawater prepared with Tropic of Marin Salts.

340

341 **Reporter plasmid design and molecular cloning**

342 Dataset S1 lists the complete inventory of engineered plasmids with a summary of
343 primers, cloning methods, and annotations for constructing each plasmid. Complete plasmid
344 sequences and plasmids have also been deposited at Addgene
345 (http://www.addgene.org/Nicole_King). Below is a brief summary of considerations for designing
346 plasmids, and a more detailed description of standard molecular cloning methods for
347 engineering plasmids can be found in the Supplementary Information.

348 **Cloning regulatory regions from *S. rosetta* genes.** Because we had no previous
349 knowledge about the architecture of choanoflagellate regulatory regions, we aimed to clone as

350 much as 1000 bp upstream and downstream of targeted open reading frames as these
351 fragments are slightly larger than the mean intergenic distance of 885 bp (Sebe-Pedros *et al.*,
352 2017). Of necessity, the cloned intergenic sequences reported here were shorter to avoid
353 repetitive CA and GT sequences that were present before the putative promoter and after the
354 3'-UTR, respectively. To increase the specificity of primers, we designed the primers to anneal
355 to regions with a GC content ≤ 50%, as the *S. rosetta* genome is 56% GC. Ultimately, the
356 cloned regions that encompass the promoter and the 5'-UTR ranged in size from 550 bp to
357 1095 bp and those encompassing the 3'UTR ranged from 200 bp to 807 bp.
358 **Synthetic gene design.** Synthetic reporter genes (*nanoluc* and the genes encoding
359 diverse fluorescent proteins listed in Supplementary File 1) were codon optimized to match the
360 codon usage of the set of highly expressed intron-less genes listed in Fig. S1, as codon usage
361 can be biased for highly expressed genes (Hiraoka *et al.*, 2009). A codon usage table (Dataset
362 S2) was generated from the coding sequences of highly expressed intronless genes (Dataset
363 S2A) and from all coding sequences (Dataset S2B) using the 'cusp' tool in Emboss (Rice *et al.*,
364 2000). The codon usage table was then used to generate a codon optimized DNA sequence for
365 each target protein sequence with the 'backtranseq' tool on Emboss. The DNA sequences were
366 further edited by making synonymous substitutions with less frequently used codons to change
367 restriction enzyme sites and to remove repetitive sequences. Finally, sequences were added to
368 the ends of these designed genes for cloning with restriction enzymes or Gibson assembly. The
369 engineered reporter gene sequences are available through Addgene (Dataset S1;
370 http://www.addgene.org/Nicole_King).
371 **Subcellular marker design.** Dataset S3 provides the amino acid sequences for all of the
372 subcellular markers reported in Fig. 3. To ensure that the fluorescent protein tag for each
373 marker would not interfere with the functions of proteins or peptides that determine localization,
374 some of the constructs were engineered to have a flexible linker sequence (SGGSGGS)
375 separating the fluorescent protein and the localization signals.
376
377 **Optimized transfection protocol**
378 The protocol is summarized in Fig. 2 and detailed protocols for reagent preparation and
379 transfection are available at protocols.io at the following link:
380 http://www.protocols.io/groups/king-lab
381 **Culture.** Two days prior to transfection, a culture flask (Corning, Cat. No. 353144) was
382 seeded with *S. rosetta* at a density of 5,000 cells/ml in 200 ml of 1x High Nutrient Media. The

383 culture was supplemented with 2 mg of frozen *E. pacifica* by resuspending a 10 mg pellet of
384 flash-frozen *E. pacifica* in 1 ml of media and then adding 200 μl of the resuspended pellet to the
385 culture of *S. rosetta*.

386 **Wash.** After 36-48 hours of growth, bacteria were washed away from *S. rosetta* cells
387 through three consecutive rounds of centrifugation and resuspension in sterile AK seawater.
388 The culture flask was vigorously shaken for 30 sec to homogenize the 200 ml that was seeded
389 two days prior (see above) and then transferred to 50 ml conical tubes and spun for 5 min at
390 2000 x g and 22°C. The supernatant was removed with a serological pipette, and residual
391 media was removed with a fine tip transfer pipette. The cell pellets were resuspended in a total
392 volume of 100 ml of AK seawater, vigorously shaken in their conical tubes for 30 sec, and then
393 centrifuged for 5 min at 2200 x g and 22°C. The supernatant was removed as before. Each cell
394 pellet was resuspended in 50 ml of AK seawater, vigorously shaken for 30 sec, and centrifuged
395 for 5 min at 2400 x g and 22°C. After the supernatant was removed, the cells were resuspended
396 in a total volume of 100 μl of AK seawater. A 100-fold dilution of cells was counted on a Luna-FL
397 automated cell counter (Logos Biosystems) and the remaining cells were diluted to a final
398 concentration of $5x10^7$ choanoflagellate cells/ml. The resuspended cells were divided into 100 μl
399 aliquots with $5x10^6$ cells per aliquot to immediately prime cells in the next step. A 200 ml culture
400 typically yields 6-8 aliquots of cells.

401 **Prime.** After washing away bacteria, each aliquot of *S. rosetta* cells was incubated in
402 priming buffer to remove the extracellular material coating the cell. The 100 μl aliquots that
403 contained $5x10^6$ cells were centrifuged for 5 min at 800 x g and at room temperature. The
404 supernatant was removed with a fine tip micropipette. Cells were resuspended in 100 μl of
405 priming buffer (40 mM HEPES-KOH, pH 7.5; 34 mM Lithium Citrate; 50 mM L-Cysteine; 15%
406 (w/v) PEG 8000; and 1 μM papain) and then incubated for 30 min. Priming was quenched by
407 adding 2 μl of 50 mg/ml bovine serum albumin-fraction V (Sigma) and then centrifuged for 5 min
408 at 1250 x g and 22°C with the centrifuge brake set to a 'soft' setting. The supernatant was
409 removed with a fine-tip micropipette, and the cells were resuspended in 25 μl of SF Buffer
410 (Lonza).

411 **Nucleofect.** Each transfection reaction was prepared by adding 2 μl of 'primed' cells
412 resuspended in SF buffer to a mixture of 14 μl of SF Buffer; 2 μl of 20 μg/μl pUC19; 1 μl of 250
413 mM ATP, pH 7.5; 1 μl of 100 mg/ml Sodium Heparin; and ≤7 μl of reporter DNA. (Note that
414 higher volumes of nucleofection lead to lower transfection frequencies; thus, reporter DNA
415 should be as concentrated as possible, not exceeding 7 μl. Also, see below for "Note about

416 titrating reporter plasmids.”) The transfection reaction was transferred to one well of a 96-well
417 nucleofection plate (Lonza). The nucleofection plate was placed in a Nucleofector 4d 96-well
418 Nucleofection unit (Lonza), and the CM156 pulse was applied to each well.
419 **Rest and recover.** Immediately after pulsation, 100 μl of ice-cold recovery buffer (10 mM
420 HEPES-KOH, pH 7.5; 0.9 M Sorbitol; 8% (w/v) PEG 8000) was added to the cells, Recovery
421 buffer was gently mixed with the transfected cells by firmly tapping the side of the plate and then
422 incubating the samples for 5 min. The whole volume of the transfection reaction plus the
423 recovery buffer was transferred to 1 ml of 1x High Nutrient Media in a 12-well plate. After the
424 cells recovered for 1 hour, 5 μl of a 10 mg frozen *E. pacifica* pellet resuspended in media (see
425 above), was added to each well. The cells were grown for 24 to 48 hours before assaying for
426 luminescence or fluorescence.
427 **Note about establishing transfection in non-model microeukaryotes.** Establishing a
428 transfection protocol for *S. rosetta* required adapting several different transfection procedures
429 for a variety of eukaryotic cells to meet the unique requirements of *S. rosetta*. While the specific
430 details for transfecting *S. rosetta* may not be readily applicable to other organisms, the general
431 considerations and the process for optimization that led to the development of the transfection
432 protocol described here could inform efforts to transfect other microeukaryotes. Therefore, we
433 have included a summary in the supplementary information (See text and Figs. S10 and S11) of
434 the initial development and optimization of the aforementioned protocol.
435
436 **Nanoluc reporter assay**
437 To measure relative transfection efficiency resulting from different transfection protocols
438 and promoters, we performed luciferase assays on lysates of transfected cells. Cells transfected
439 with 2.5 μg of *nanoluc* reporter plasmids were pelleted by centrifuging for 10 min at 4200 x g
440 and 4°C. The supernatant was removed and the cells were resuspended in 50 μl of NanoGlo
441 buffer (Promega) and then transferred to a well of a white, opaque 96-well plate (Greiner Bio-
442 one Cat No.655083). Luminescence was immediately recorded on a Spectramax L Microplate
443 Reader (Molecular Devices) with a 1 min dark adaption and 10 sec dwell time with the
444 photomultiplier gain set to photon counting mode.
445 Based on standard definitions from analytical chemistry (Harris, 2007) the detection limit
446 was set to three standard deviations above the background signal such that any signal above
447 the detection limit has less than a 1% chance of arising from random error. The limit of detection
448 was calculated in two different ways. First, the y-axis intercept and standard deviation were

449 calculated from a standard curve (Harris, 2007) fit to a serial dilution of nanoluc versus
450 luciferase activity (Fig. S3A). To decrease the bias toward higher luciferase values, the standard
451 curve was fit with the objective *(O)*: $O \equiv \min \sum_i \frac{|m_i - c_i|}{m_i}$, where *m* is the measured luciferase value
452 for a given data point *i* and *c* is the calculated luciferase value. Second, the detection limit was
453 also determined as three standard deviations above the mean of eight replicate luciferase
454 measurements of cells transfected without any reporter plasmid, which resulted in the same
455 calculated detection limit.
456 Reproducibility in luciferase assays was assessed by performing at least two independent
457 experiments on separate days with different preparations of 'primed' cells; data presented in
458 Fig. 2, S2, S3, S10, and S11 represent one of the independent experiments. Within each
459 experiment from the same preparation of 'primed' cells, replicate measurements were
460 performed by setting up three to five independent transfections for each condition (shown as
461 black dots); bar graphs in Fig. 2, S2, S3, S10, and S11 show the mean values of the five
462 independent transfections with error bars showing the standard deviation. Before performing
463 statistical tests that rely on a normal distribution, luciferase data were transformed to a log-
464 normal distribution by taking the base-10 logarithm of luciferase values as gene expression data
465 from luciferase assays display a log-normal distribution (Muranaka *et al.*, 2013).
466
467 **Flow Cytometry**
468 To measure the percentage of cells expressing each of the different transgenes under
469 different transfection conditions, we used flow cytometry. Cells were transfected with 10 *μ*g of
470 mWasabi or 10 *μ*g of TagRFP-T reporter plasmids for flow cytometry because these
471 fluorophores produced the highest fluorescence signal upon illumination with the 488 or 561 nm
472 lasers, respectively. To prepare cells for flow cytometry, cultures from 10-12 transfections were
473 pooled 24 hours after transfection and centrifuged for 15 min at 3600 x g and 4°C. The
474 supernatant was removed with a fine-tip transfer pipette to avoid disturbing the pellet. The
475 pelleted cells were resuspended in 500 *μ*l of 0.22 *μ*m filtered AK seawater and then filtered
476 through a 40 *μ*m filter.
477 Because a large number of bacteria were present in the cultures, *S. rosetta* cells were
478 gated based on the area of forward scattering signal versus the area of the side scattering
479 signal and the area of the forward scattering signal versus the height of the forward scattering
480 signals. To differentiate transfected cells from untransfected cells, fluorescence signal was

481 measured using lasers and filters for the fluorophores FITC (Green Fluorescence) and PE (Red
482 Fluorescence); untransfected cells form a population along the y=x line of these plots, and the
483 population of transfected cells are skewed along one axis that corresponds to the fluorophore.
484 The transfected cells were gated to exclude >99.99% of untransfected cells as determined from
485 a negative control reaction that was transfected without a fluorescent reporter (Fig. 2E, left
486 panel).
487
488 **Live cell imaging**
489 An important benefit of transgenics is the ability to visualize protein localization and cell
490 architecture in living cells. To this end, we have established improved protocols for live cell
491 imaging in *S. rosetta*. Glass-bottomed dishes were prepared for live cell microscopy by corona-
492 treating the glass for 10 s. Afterwards, 300 μl of 0.1 mg/ml poly-D-lysine was applied to the
493 glass cover (18 μl/cm^2), incubated for 10 min at room temperature, and then removed. Excess
494 poly-D-lysine was washed away from the glass surface with three rinses of 500 μl artificial
495 seawater.
496 Cells transfected with 5 μg of each fluorescent reporter were prepared for microscopy by
497 centrifuging 1-2 ml of transfected cells for 10 min at 3,600 x g and 4°C. After centrifugation, the
498 supernatant was removed and the cell pellet was resuspended in 200 μl of 4/5 Tropic of Marin
499 artificial seawater with 100 mM LiCl. Lithium chloride slows flagellar beating, as in spermatozoa
500 (Brokaw, 1987; Gibbons and Gibbons, 2013), to decrease the movement of cells during
501 imaging. The resuspended cells were pipetted on top of the poly-D-lysine coated glass-bottom
502 dish and adsorbed on the surface for 10 min. Lastly, 200 μl of 20% (w/v) Ficoll 400 dissolved in
503 4/5 Tropic of Marin artificial seawater with 100 mM LiCl was pipetted drop-by-drop on top of the
504 cells. The addition of Ficoll decreases flagellar movement by increasing the viscosity of the
505 media (Wilson *et al.*, 2015; Pate and Brokaw, 1980) without significantly changing the
506 osmolarity or refractive index of the sample (GE Lifesciences).
507 Confocal microscopy was performed on a Zeiss Axio Observer LSM 880 with an Airyscan
508 detector and a 63x/NA1.40 Plan-Apochromatic oil immersion objective. The mTFP1 and
509 mCherry fluorophores were selected for two-color imaging due to their high photostability and
510 minimal spectral overlap. Confocal stacks were acquired in superresolution mode using ILEX
511 line scanning and two-fold averaging and the following settings: 40 nm x 40 nm pixel size, 93
512 nm z-step, 0.9-1.0 μsec/pixel dwell time, 850 gain, 458 nm laser operating at 5% laser power,
513 561 nm laser operating at 3% laser power, 458/561 nm multiple beam splitter, and 495-550 nm

514 band-pass/570 nm long-pass filter. Images were initially processed using the automated
515 Airyscan algorithm (Zeiss) and then reprocessed by setting the Airyscan threshold 0.5 units
516 higher than the value reported from automated Airyscan processing. The stacks were further
517 processed by correcting for signal decay, background, and flickr in Zen Blue (Zeiss). Last, FIJI
518 (Schindelin *et al.*, 2012) was used to apply a gamma factor to each channel and subtract the
519 background using a 100 pixel radius.
520 Epifluorescence and differential interference contrast images were recorded using a Zeiss
521 Axio Observer.Z1/7 Widefield microscope with a Hamamatsu Orca-Flash 4.0 LT CMOS Digital
522 Camera and 40x/NA 1.1 LD C-Apochromatic water immersion, 63x/NA1.40 Plan-Apochromatic
523 oil immersion, or 100x NA 1.40 Plan-Apochromatic oil immersion objectives. Green fluorescent
524 proteins were imaged with a 38 HE filter set and red fluorescent proteins with a 43 HE filter set.
525 Images were processed by applying a gamma factor and background subtracting fluorescence
526 channels in FIJI.
527 **Note about titrating reporter plasmids.** A titration of fluorescent reporter plasmids
528 showed that 10 μg of total reporter plasmid(s) best balanced transfection efficiency, brightness,
529 and a faithful indication of subcellular architecture. We caution that high plasmid concentrations
530 can result in the overexpression of fluorescent markers, leading to aberrant localization of the
531 marker and gross changes in cell morphology. Such artefacts can be avoided by performing a
532 titration to determine the best concentration of plasmid and recording images from cells with a
533 range of fluorescence intensities that result from any transfection. One of the best markers to
534 assess optimal reporter plasmid concentrations is the tubulin marker because of its distinct
535 localization that can be benchmarked with immunofluorescence.
536
537 **Immunofluorescence staining and imaging**
538 Immunfluorescence was performed as previously described (Woznica *et al.*, 2016) with
539 modifications to better preserve features of the cytoskeleton. Two milliliters of cells were
540 concentrated by centrifugation for 10 min at 2750 x g and 4°C. The cells were resuspended in
541 400 μl of artificial seawater and applied to poly-L-lysine coated coverslips (BD Biosciences)
542 placed in the bottom of each well of a 24-well cell culture dish. After allowing the cells to settle
543 on the coverslip for 30 min, 150 μl of the cell solution was gently removed from the side of the
544 dish. It is crucial to leave a small layer of buffer on top of cells to preserve the cell morphology,
545 hence the 250 μl of liquid left in the well. All of the subsequent washes and incubations during
546 the staining procedure were performed by adding and removing 200 μl of the indicated buffer.

547 Cells were fixed in two stages. First, the coverslip was washed once with 6% acetone in
548 cytoskeleton buffer (10 mM MES, pH 6.1; 138 KCl, 3 mM $MgCl_2$; 2 mM EGTA; 675 mM
549 Sucrose), which better preserves the actin cytoskeleton (Cramer and Mitchison, 1995; Symons
550 and Mitchison, 1991), and then incubated for 10 min at room temperature after a second
551 application of the acetone solution. Subsequently, the coverslip was washed once with 4%
552 formaldehyde diluted in cytoskeleton buffer and then incubated for 15 min at room temperature
553 after a second application of the formaldehyde solution. Last, the coverslip was gently washed
554 three times with cytoskeleton buffer.
555 Cells were permeabilized by washing the coverslip once with permeabilization buffer (100
556 mM PIPES, pH 6.95; 2 mM EGTA; 1 mM $MgCl_2$; 1% (w/v) bovine serum albumin-fraction V;
557 0.3% (v/v Triton X-100) and then incubated for 30 min upon a second addition of
558 permeabilization buffer. After the permeabilization buffer was removed, the coverslip was
559 washed once with primary antibody, 50 ng/ml mouse E7 anti-tubulin antibody (Developmental
560 Studies Hybridoma Bank) diluted in permeabilization buffer, and then incubated for 1 h in a
561 second application of primary antibody. The coverslip was gently washed twice in
562 permeabilization buffer. Next, the coverslip was washed once with secondary antibody, 8 ng/ml
563 Donkey anti-mouse IgG–AlexaFluor568 (ThermoFisher) diluted in permeabilization buffer, and
564 then incubated for 1 h after a second application of secondary antibody. Afterwards, the
565 coverslip was washed once in permeabilization buffer and then three times with PEM (100 mM
566 PIPES-KOH, pH 6.95; 2 mM EGTA; 1 mM $MgCl_2$). The coverslip was washed once with 10
567 μg/ml Hoechst 33342 and 4 U/ml Phalloidin-AlexaFluor488 in PEM and then incubated for 30
568 min with a second application of Hoechst33342/Phalloidin. Finally, the coverslip was washed
569 once in PEM.
570 To prepare a slide for mounting, 10 μl of Pro-Long Diamond (Invitrogen) was added to a
571 slide. The coverslip was gently removed from the well with forceps, excess buffer was blotted
572 from the side with a piece of filter paper, and the coverslip was gently placed on the drop of Pro-
573 Long diamond. The mounting media was allowed to cure overnight before visualization.
574 Images were acquired on a Zeiss LSM 880 Airyscan confocal microscope with a 63x
575 objective (as described for live cell imaging) by frame scanning in the superresolution mode with
576 the following settings: 35 nm x 35 nm pixel size; 80 nm z-step; 0.64 μs/pixel dwell time; 561 nm
577 laser operating at 1.5% power with a 488/561 nm beam splitter, a 420-480 nm/495-620 nm
578 band pass filter, and a gain of 750; 488 nm laser operating at 1.5% power with a 488/561 nm
579 beam splitter, a 420-480 nm/495-550 nm band pass filter, and a gain of 750; and 405 nm laser

580 operating at 1.5% power with a 405 nm beam splitter, a 420-480 nm/495-550 nm band pass
581 filter, and a gain of 775.
582

Acknowledgements

Laura Wetzel, Monika Sigg, Hannah Elzinga, Lily Helfrich, and Reef Aldayafleh helped with experiments and reagent preparation. Corey Allard, as part of the Marine Biological Laboratory's Physiology Course, helped with early tests of priming conditions. Kent McDonald generously provided a transmission electron micrograph from samples prepared by Pawel Burkhardt. We thank these people for providing access and support for scientific instruments: Russell Vance and Lab for use of their luminometer, Hector Nolla and Alma Valeros in the Flow Cytometry Facility, and the UC Berkeley DNA Sequencing Facility. The following individuals generously donated reagents and provided technical support: Brad Hook and Dee Czarniecki from Promega, Ethan Brooks from Lonza, and Colleen Manning from Zeiss. We appreciate scientific discussions and advice from these individuals: David Schaffer, Sabrina Sun, Jorge Ortiz, Niren Murthy, Tara DeBoer, Fyodor Urnov, Matt Welch and Lab, Rebecca Heald and Lab, Abby Dernberg and Lab, and Amy Gladfelter. We thank members of the King lab for helpful discussions, research support, and comments on the manuscript, especially Arielle Woznica, Kayley Hake, and Ben Larson. An additional thanks to the following people for providing comments on the manuscript: Candace Britton, Pawel Burkhardt, Matt Daugherty, Galo Garcia, Tera Levin, Kristin Patrick, and Dan Richter. DSB is supported as a Simons Foundation Postdoctoral Fellow of the Jane Coffin Childs Memorial Fund for Biomedical Research. This work was funded in part by a grant from the Gordon and Betty Moore Foundation's Marine Microbiology Initiative for establishing Emerging Model Systems.

Author Contributions

DSB and NK conceived of the project and wrote the manuscript. DSB, HSM, and NK designed experiments and interpreted data. DSB and HSM collected data.

607 **REFERENCES**

608 Abedin, M. and King, N. (2008). The premetazoan ancestry of cadherins. Science *5865*, 946-
609 948.

610 Adam, J. C., Pringle, J. R. and Peifer, M. (2000). Evidence for functional differentiation among
611 Drosophila septins in cytokinesis and cellularization. Mol. Biol. Cell *9*, 3123-3135.

612 Ai, H. W., Henderson, J. N., Remington, S. J. and Campbell, R. E. (2006). Directed evolution of
613 a monomeric, bright and photostable version of *Clavularia* cyan fluorescent protein: structural
614 characterization and applications in fluorescence imaging. Biochem. J. *3*, 531-540.

615 Ai, H. W., Olenych, S. G., Wong, P., Davidson, M. W. and Campbell, R. E. (2008). Hue-shifted
616 monomeric variants of *Clavularia* cyan fluorescent protein: identification of the molecular
617 determinants of color and applications in fluorescence imaging. BMC Biol., 13.

618 Alegado, R. A., Brown, L. W., Cao, S., Dermenjian, R. K., Zuzow, R., Fairclough, S. R., Clardy,
619 J. and King, N. (2012). A bacterial sulfonolipid triggers multicellular development in the closest
620 living relatives of animals. eLife, e00013.

621 Atkinson, M. J. and Bingman, C. (1998). Elemental composition of commercial seasalts. Journal
622 of Aquariculture and Aquatic Sciences *2*, 39-43.

623 Barral, Y., Mermall, V., Mooseker, M. S. and Snyder, M. (2000). Compartmentalization of the
624 cell cortex by septins is required for maintenance of cell polarity in yeast. Mol. Cell *5*, 841-851.

625 Berepiki, A. and Read, N. D. (2013). Septins are important for cell polarity, septation and
626 asexual spore formation in *Neurospora crassa* and show different patterns of localisation at
627 germ tube tips. PLoS One *5*, e63843.

628 Bertin, A., McMurray, M. A., Grob, P., Park, S. S., Garcia, G., Patanwala, I., Ng, H. L., Alber, T.,
629 Thorner, J. and Nogales, E. (2008). *Saccharomyces cerevisiae* septins: supramolecular
630 organization of heterooligomers and the mechanism of filament assembly. Proc. Natl. Acad. Sci.
631 U. S. A. *24*, 8274-8279.

632 Bertin, A., McMurray, M. A., Thai, L., Garcia, G., Votin, V., Grob, P., Allyn, T., Thorner, J. and
633 Nogales, E. (2010). Phosphatidylinositol-4,5-bisphosphate promotes budding yeast septin
634 filament assembly and organization. J. Mol. Biol. *4*, 711-731.

635 Bowen, J. R., Hwang, D., Bai, X., Roy, D. and Spiliotis, E. T. (2011). Septin GTPases spatially
636 guide microtubule organization and plus end dynamics in polarizing epithelia. J. Cell Biol. *2*,
637 187-197.

638 Bridges, A. A., Jentzsch, M. S., Oakes, P. W., Occhipinti, P. and Gladfelter, A. S. (2016).
639 Micron-scale plasma membrane curvature is recognized by the septin cytoskeleton. J. Cell Biol.
640 *1*, 23-32.

641 Bridges, A. A., Zhang, H., Mehta, S. B., Occhipinti, P., Tani, T. and Gladfelter, A. S. (2014).
642 Septin assemblies form by diffusion-driven annealing on membranes. Proc. Natl. Acad. Sci. U.
643 S. A. *6*, 2146-2151.

644 Brokaw, C. J. (1987). A lithium-sensitive regulator of sperm flagellar oscillation is activated by
645 cAMP-dependent phosphorylation. J. Cell Biol. *4*, 1789-1798.

646 Brunet, T. and King, N. (2017). The Origin of Animal Multicellularity and Cell Differentiation.
647 Dev. Cell. *2*, 124-140.

648 Burger, G., Forget, L., Zhu, Y., Gray, M. W. and Lang, B. F. (2003). Unique mitochondrial
649 genome architecture in unicellular relatives of animals. Proc. Natl. Acad. Sci. U. S. A. *3*, 892-
650 897.

651 Burkhardt, P., Gronborg, M., McDonald, K., Sulur, T., Wang, Q. and King, N. (2014).
652 Evolutionary insights into premetazoan functions of the neuronal protein homer. Mol. Biol. Evol.
653 *9*, 2342-2355.

654 Cannon, K. S., Woods, B. L., Crutchley, J. M. and Gladfelter, A. S. (2018). An amphipathic helix
655 enables septins to sense micron-scale membrane curvature. bioRxiv.

656 Caro, F., Miller, M. G. and DeRisi, J. L. (2012). Plate-based transfection and culturing technique
657 for genetic manipulation of *Plasmodium falciparum*. Malar J., 22.

658 Casamayor, A. and Snyder, M. (2003). Molecular dissection of a yeast septin: distinct domains
659 are required for septin interaction, localization, and function. Mol. Cell. Biol. *8*, 2762-2777.

660 Cid, V. J., Adamikova, L., Cenamor, R., Molina, M., Sanchez, M. and Nombela, C. (1998). Cell
661 integrity and morphogenesis in a budding yeast septin mutant. Microbiology *Pt 12*, 3463-3474.

662 Cramer, L. P. and Mitchison, T. J. (1995). Myosin is involved in postmitotic cell spreading. J.
663 Cell Biol. *1*, 179-189.

664 Dayel, M. J., Alegado, R. A., Fairclough, S. R., Levin, T. C., Nichols, S. A., McDonald, K. and
665 King, N. (2011). Cell differentiation and morphogenesis in the colony-forming choanoflagellate
666 *Salpingoeca rosetta*. Dev. Biol. *1*, 73-82.

667 Dayel, M. J. and King, N. (2014). Prey capture and phagocytosis in the choanoflagellate
668 *Salpingoeca rosetta*. PLoS One *5*, e95577.

669 Fairclough, S. R. *et al.* (2013). Premetazoan genome evolution and the regulation of cell
670 differentiation in the choanoflagellate *Salpingoeca rosetta*. Genome Biol. *2*, r15.

671 Fairclough, S. R., Dayel, M. J. and King, N. (2010). Multicellular development in a
672 choanoflagellate. Curr. Biol. *20*, 875.

673 Fares, H., Peifer, M. and Pringle, J. R. (1995). Localization and possible functions of *Drosophila*
674 septins. Mol. Biol. Cell *12*, 1843-1859.

675 Ford, S. K. and Pringle, J. R. (1991). Cellular morphogenesis in the *Saccharomyces cerevisiae*
676 cell cycle: localization of the CDC11 gene product and the timing of events at the budding site.
677 Dev. Genet. *4*, 281-292.

678 Friedman, J. R., Lackner, L. L., West, M., DiBenedetto, J. R., Nunnari, J. and Voeltz, G. K.
679 (2011). ER tubules mark sites of mitochondrial division. Science *6054*, 358-362.

680 Garcia, G., Bertin, A., Li, Z., Song, Y., McMurray, M. A., Thorner, J. and Nogales, E. (2011).
681 Subunit-dependent modulation of septin assembly: budding yeast septin Shs1 promotes ring
682 and gauze formation. J. Cell Biol. *6*, 993-1004.

683 Gibbons, B. H. and Gibbons, I. R. (2013). Lithium reversibly inhibits microtubule-based motility
684 in sperm flagella. Nature *5968*, 560-562.

685 Gresch, O. *et al.* (2004). New non-viral method for gene transfer into primary cells. Methods *2*,
686 151-163.

687 Haarer, B. K. and Pringle, J. R. (1987). Immunofluorescence localization of the *Saccharomyces*
688 *cerevisiae* CDC12 gene product to the vicinity of the 10-nm filaments in the mother-bud neck.
689 Mol. Cell. Biol. *10*, 3678-3687.

690 Hall, M. P. *et al.* (2012). Engineered luciferase reporter from a deep sea shrimp utilizing a novel
691 imidazopyrazinone substrate. ACS Chem. Biol. *11*, 1848-1857.

692 Hallegraeff, G. M., Anderson, D. M. and Cembella, A. D. (2004). Manual on Harmful
693 Marine Microalgae, Paris, France: United Nations Educational, Scientific and Cultural
694 Organization.

695 Hamm, A., Krott, N., Breibach, I., Blindt, R. and Bosserhoff, A. K. (2002). Efficient transfection
696 method for primary cells. Tissue Eng. *2*, 235-245.

697 Harris, D. C. (2007). Quantitative chemical analysis, New York, NY: W.H. Freeman and Co.

698 Hartwell, L. H. (1971). Genetic control of the cell division cycle in yeast. IV. Genes controlling
699 bud emergence and cytokinesis. Exp. Cell Res. *2*, 265-276.

700 Helfer, H. and Gladfelter, A. S. (2006). AgSwe1p regulates mitosis in response to
701 morphogenesis and nutrients in multinucleated *Ashbya gossypii* cells. Mol. Biol. Cell *10*, 4494-
702 4512.

703 Hiraoka, Y., Kawamata, K., Haraguchi, T. and Chikashige, Y. (2009). Codon usage bias is
704 correlated with gene expression levels in the fission yeast *Schizosaccharomyces pombe*. Genes
705 Cells *4*, 499-509.

706 Hoi, H., Howe, E. S., Ding, Y., Zhang, W., Baird, M. A., Sell, B. R., Allen, J. R., Davidson, M. W.
707 and Campbell, R. E. (2013). An engineered monomeric *Zoanthus* sp. yellow fluorescent protein.
708 Chem. Biol. *10*, 1296-1304.

709 Hu, Q., Milenkovic, L., Jin, H., Scott, M. P., Nachury, M. V., Spiliotis, E. T. and Nelson, W. J.
710 (2010). A septin diffusion barrier at the base of the primary cilium maintains ciliary membrane
711 protein distribution. Science *5990*, 436-439.

712 Huang, Y. W., Yan, M., Collins, R. F., Diciccio, J. E., Grinstein, S. and Trimble, W. S. (2008).
713 Mammalian septins are required for phagosome formation. Mol. Biol. Cell *4*, 1717-1726.

714 Huh, W. K., Falvo, J. V., Gerke, L. C., Carroll, A. S., Howson, R. W., Weissman, J. S. and
715 O'Shea, E. K. (2003). Global analysis of protein localization in budding yeast. Nature *6959*, 686-
716 691.

717 James-Clark, H. (1868). On the Spongiae Ciliatae as Infusoria Flagellata: or observations on the
718 structure, animality and relationship of *Leucosolenia botryoides* Bowerbank. The Annals and
719 Magazine of Natural History, 250–64.

720 Janse, C. J., Franke-Fayard, B., Mair, G. R., Ramesar, J., Thiel, C., Engelmann, S.,
721 Matuschewski, K., van Gemert, G. J., Sauerwein, R. W. and Waters, A. P. (2006). High
722 efficiency transfection of *Plasmodium berghei* facilitates novel selection procedures. Mol.
723 Biochem. Parasitol. *1*, 60-70.

724 Janse, C. J., Ramesar, J. and Waters, A. P. (2006). High-efficiency transfection and drug
725 selection of genetically transformed blood stages of the rodent malaria parasite *Plasmodium*
726 *berghei*. Nat. Protoc. *1*, 346-356.

727 Kalderon, D., Roberts, B. L., Richardson, W. D. and Smith, A. E. (1984). A short amino acid
728 sequence able to specify nuclear location. Cell *3 Pt 2*, 499-509.

729 Kanda, T., Sullivan, K. F. and Wahl, G. M. (1998). Histone-GFP fusion protein enables sensitive
730 analysis of chromosome dynamics in living mammalian cells. Curr. Biol. *7*, 377-385.

731 Karpov, S. A. and Leadbeater, B. S. C. (1998). Cytoskeleton Structure and Composition in
732 Choanoflagellates. J. Eukaryot. Microbiol. *3*, 361-367.

733 Kawai, S., Hashimoto, W. and Murata, K. (2010). Transformation of *Saccharomyces cerevisiae*
734 and other fungi: methods and possible underlying mechanism. Bioeng. Bugs *6*, 395-403.

735 Kent, W. S. (1871). Affinities of the sponges. Nature. *4*, 184.

736 Kim, H. B., Haarer, B. K. and Pringle, J. R. (1991). Cellular morphogenesis in the
737 *Saccharomyces cerevisiae* cell cycle: localization of the CDC3 gene product and the timing of
738 events at the budding site. J. Cell Biol. *4*, 535-544.

739 Kim, J. and Cooper, J. A. (2018). Septins regulate junctional integrity of endothelial monolayers.
740 Mol. Biol. Cell *13*, 1693-1703.

741 Kim, S. K. *et al.* (2010). Planar cell polarity acts through septins to control collective cell
742 movement and ciliogenesis. Science *5997*, 1337-1340.

743 King, N. (2004). The unicellular ancestry of animal development. Dev. Cell. *3*, 313-325.

744 King, N., Hittinger, C. T. and Carroll, S. B. (2003). Evolution of key cell signaling and adhesion
745 protein families predates animal origins. Science *5631*, 361-363.

746 King, N. *et al.* (2008). The genome of the choanoflagellate *Monosiga brevicollis* and the origin of
747 metazoans. Nature *7180*, 783-788.

748 King, N., Young, S. L., Abedin, M., Carr, M. and Leadbeater, B. S. (2009). Visualizing the
749 subcellular localization of actin, beta-tubulin, and DNA in *Monosiga brevicollis*. Cold Spring Harb
750 Protoc. *2*, pdb.prot5150.

751 Kremer, B. E., Haystead, T. and Macara, I. G. (2005). Mammalian septins regulate microtubule
752 stability through interaction with the microtubule-binding protein MAP4. Mol. Biol. Cell *10*, 4648-
753 4659.

754 Kusch, J., Meyer, A., Snyder, M. P. and Barral, Y. (2002). Microtubule capture by the cleavage
755 apparatus is required for proper spindle positioning in yeast. Genes Dev. *13*, 1627-1639.

756 Lang, B. F., O'Kelly, C., Nerad, T., Gray, M. W. and Burger, G. (2002). The closest unicellular
757 relatives of animals. Curr. Biol. *20*, 1773-1778.

758 Leadbeater, B. S. C. (2015). The Choanoflagellates: Evolution, Biology and Ecology,
759 Cambridge, United Kingdom: Cambridge University Press.

760 Levin, T. C., Greaney, A. J., Wetzel, L. and King, N. (2014). The rosetteless gene controls
761 development in the choanoflagellate *S. rosetta*. eLife, e04070.

762 Levin, T. C. and King, N. (2013). Evidence for sex and recombination in the choanoflagellate
763 *Salpingoeca rosetta*. Curr. Biol. *21*, 2176-2180.

764 Li, R., Neundorf, I. and Nitsche, F. (2018). First Efficient Transfection in Choanoflagellates using
765 Cell-Penetrating Peptides. bioRxiv.

766 Manning, G., Young, S. L., Miller, W. T. and Zhai, Y. (2008). The protist, *Monosiga brevicollis*,
767 has a tyrosine kinase signaling network more elaborate and diverse than found in any known
768 metazoan. Proc. Natl. Acad. Sci. U. S. A. *28*, 9674-9679.

769 Mavrakis, M., Azou-Gros, Y., Tsai, F. C., Alvarado, J., Bertin, A., Iv, F., Kress, A., Brasselet, S.,
770 Koenderink, G. H. and Lecuit, T. (2014). Septins promote F-actin ring formation by crosslinking
771 actin filaments into curved bundles. Nat. Cell Biol. *4*, 322-334.

772 McMurray, M. A., Bertin, A., Garcia, G., Lam, L., Nogales, E. and Thorner, J. (2011). Septin
773 filament formation is essential in budding yeast. Dev. Cell. *4*, 540-549.

774 Meads, T. and Schroer, T. A. (1995). Polarity and nucleation of microtubules in polarized
775 epithelial cells. Cell Motil. Cytoskeleton *4*, 273-288.

776 Meseroll, R. A., Howard, L. and Gladfelter, A. S. (2012). Septin ring size scaling and dynamics
777 require the coiled-coil region of Shs1p. Mol. Biol. Cell *17*, 3391-3406.

778 Muranaka, T., Kubota, S. and Oyama, T. (2013). A single-cell bioluminescence imaging system
779 for monitoring cellular gene expression in a plant body. Plant Cell Physiol. *12*, 2085-2093.

780 Neufeld, T. P. and Rubin, G. M. (1994). The *Drosophila* peanut gene is required for cytokinesis
781 and encodes a protein similar to yeast putative bud neck filament proteins. Cell *3*, 371-379.

782 Nishihama, R., Onishi, M. and Pringle, J. R. (2011). New insights into the phylogenetic
783 distribution and evolutionary origins of the septins. Biol. Chem. *8-9*, 681-687.

784 Nunnari, J., Marshall, W. F., Straight, A., Murray, A., Sedat, J. W. and Walter, P. (1997).
785 Mitochondrial transmission during mating in *Saccharomyces cerevisiae* is determined by
786 mitochondrial fusion and fission and the intramitochondrial segregation of mitochondrial DNA.
787 Mol. Biol. Cell *7*, 1233-1242.

788 O'Neill, R. S. and Clark, D. V. (2013). The *Drosophila melanogaster* septin gene Sep2 has a
789 redundant function with the retrogene Sep5 in imaginal cell proliferation but is essential for
790 oogenesis. Genome *12*, 753-758.

791 Pan, F., Malmberg, R. L. and Momany, M. (2007). Analysis of septins across kingdoms reveals
792 orthology and new motifs. BMC Evol. Biol., 103.

793 Parfrey, L. W., Lahr, D. J., Knoll, A. H. and Katz, L. A. (2011). Estimating the timing of early
794 eukaryotic diversification with multigene molecular clocks. Proc. Natl. Acad. Sci. U. S. A. *33*,
795 13624-13629.

796 Park, T. J., Kim, S. K. and Wallingford, J. B. (2015). The planar cell polarity effector protein
797 Wdpcp (Fritz) controls epithelial cell cortex dynamics via septins and actomyosin. Biochem.
798 Biophys. Res. Commun. *2*, 562-566.

799 Parra-Acero, H., Ros-Rocher, N., Perez-Posada, A., Kożyczkowska, A., Sánchez-Pons, N.,
800 Nakata, A., Suga, H., Najle, S. R. and Ruiz-Trillo, I. (2018). Transfection of *Capsaspora*
801 *owczarzaki*, a close unicellular relative of animals. Development.

802 Pate, E. F. and Brokaw, C. J. (1980). Movement of spermatozoa in viscous environments. J.
803 Exp. Biol., 395-397.

804 Pedelacq, J. D., Cabantous, S., Tran, T., Terwilliger, T. C. and Waldo, G. S. (2006). Engineering
805 and characterization of a superfolder green fluorescent protein. Nat. Biotechnol. *1*, 79-88.

806 Reid, T. S., Terry, K. L., Casey, P. J. and Beese, L. S. (2004). Crystallographic analysis of CaaX
807 prenyltransferases complexed with substrates defines rules of protein substrate selectivity. J.
808 Mol. Biol. *2*, 417-433.

809 Rice, P., Longden, I. and Bleasby, A. (2000). EMBOSS: the European Molecular Biology Open
810 Software Suite. Trends Genet. *6*, 276-277.

811 Richter, D., Fozouni, P., Eisen, M. and King, N. (2018). Gene family innovation, conservation
812 and loss on the animal stem lineage. eLife, e34226.

813 Riedl, J. *et al.* (2008). Lifeact: a versatile marker to visualize F-actin. Nat. Methods *7*, 605-607.

814 Rodriguez-Boulan, E. and Macara, I. G. (2014). Organization and execution of the epithelial
815 polarity programme. Nat. Rev. Mol. Cell Biol. *4*, 225-242.

816 Rols, M. P. and Teissie, J. (1990). Modulation of electrically induced permeabilization and fusion
817 of Chinese hamster ovary cells by osmotic pressure. Biochemistry *19*, 4561-4567.

818 Rols, M. P. and Teissie, J. (1989). Ionic-strength modulation of electrically induced
819 permeabilization and associated fusion of mammalian cells. Eur. J. Biochem. *1*, 109-115.

820 Ruiz-Trillo, I., Roger, A. J., Burger, G., Gray, M. W. and Lang, B. F. (2008). A phylogenomic
821 investigation into the origin of metazoa. Mol. Biol. Evol. *4*, 664-672.

822 Schiestl, R. H. and Gietz, R. D. (1989). High efficiency transformation of intact yeast cells using
823 single stranded nucleic acids as a carrier. Curr. Genet. *5-6*, 339-346.

824 Schindelin, J. *et al.* (2012). Fiji: an open-source platform for biological-image analysis. Nat.
825 Methods *7*, 676-682.

826 Sebe-Pedros, A., Burkhardt, P., Sanchez-Pons, N., Fairclough, S. R., Lang, B. F., King, N. and
827 Ruiz-Trillo, I. (2013). Insights into the origin of metazoan filopodia and microvilli. Mol. Biol. Evol.
828 *9*, 2013-2023.

829 Sebe-Pedros, A., Degnan, B. M. and Ruiz-Trillo, I. (2017). The origin of Metazoa: a unicellular
830 perspective. Nat. Rev. Genet. *8*, 498-512.

831 Sellin, M. E., Holmfeldt, P., Stenmark, S. and Gullberg, M. (2011). Microtubules support a disk-
832 like septin arrangement at the plasma membrane of mammalian cells. Mol. Biol. Cell *23*, 4588-
833 4601.

834 Shaner, N. C., Campbell, R. E., Steinbach, P. A., Giepmans, B. N., Palmer, A. E. and Tsien, R.
835 Y. (2004). Improved monomeric red, orange and yellow fluorescent proteins derived from
836 *Discosoma* sp. red fluorescent protein. Nat. Biotechnol. *12*, 1567-1572.

837 Shaner, N. C. *et al.* (2013). A bright monomeric green fluorescent protein derived from
838 *Branchiostoma lanceolatum*. Nat. Methods *5*, 407-409.

839 Shaner, N. C., Lin, M. Z., McKeown, M. R., Steinbach, P. A., Hazelwood, K. L., Davidson, M. W.
840 and Tsien, R. Y. (2008). Improving the photostability of bright monomeric orange and red
841 fluorescent proteins. Nat. Methods *6*, 545-551.

842 Silverman-Gavrila, R. V., Hales, K. G. and Wilde, A. (2008). Anillin-mediated targeting of peanut
843 to pseudocleavage furrows is regulated by the GTPase Ran. Mol. Biol. Cell *9*, 3735-3744.

844 Sirajuddin, M., Farkasovsky, M., Hauer, F., Kuhlmann, D., Macara, I. G., Weyand, M., Stark, H.
845 and Wittinghofer, A. (2007). Structural insight into filament formation by mammalian septins.
846 Nature *7160*, 311-315.

847 Skelton, H. M., Burkholder, J. M. and Parrow, M. W. (2009). Axenic culture of the heterotrophic
848 dinoflagellate *Pfiesteria shumwayae* in a semi-defined medium. J. Eukaryot. Microbiol. *1*, 73-82.

849 Spiliotis, E. T. (2010). Regulation of microtubule organization and functions by septin GTPases.
850 Cytoskeleton (Hoboken) *6*, 339-345.

851 Spiliotis, E. T. and Gladfelter, A. S. (2012). Spatial guidance of cell asymmetry: septin GTPases
852 show the way. Traffic *2*, 195-203.

853 Spiliotis, E. T., Hunt, S. J., Hu, Q., Kinoshita, M. and Nelson, W. J. (2008). Epithelial polarity
854 requires septin coupling of vesicle transport to polyglutamylated microtubules. J. Cell Biol. *2*,
855 295-303.

856 Stajich, J. E., Berbee, M. L., Blackwell, M., Hibbett, D. S., James, T. Y., Spatafora, J. W. and
857 Taylor, J. W. (2009). The fungi. Curr. Biol. *18*, 840.

858 Straight, A. F., Marshall, W. F., Sedat, J. W. and Murray, A. W. (1997). Mitosis in living budding
859 yeast: anaphase A but no metaphase plate. Science *5325*, 574-578.

860 Suga, H., Dacre, M., de Mendoza, A., Shalchian-Tabrizi, K., Manning, G. and Ruiz-Trillo, I.
861 (2012). Genomic survey of premetazoans shows deep conservation of cytoplasmic tyrosine
862 kinases and multiple radiations of receptor tyrosine kinases. Sci. Signal. *222*, ra35.

863 Suga, H. and Ruiz-Trillo, I. (2013). Development of ichthyosporeans sheds light on the origin of
864 metazoan multicellularity. Dev. Biol. *1*, 284-292.

865 Symons, M. H. and Mitchison, T. J. (1991). Control of actin polymerization in live and
866 permeabilized fibroblasts. J. Cell Biol. *3*, 503-513.

867 Takizawa, P. A., DeRisi, J. L., Wilhelm, J. E. and Vale, R. D. (2000). Plasma membrane
868 compartmentalization in yeast by messenger RNA transport and a septin diffusion barrier.
869 Science *5490*, 341-344.

870 Tanaka-Takiguchi, Y., Kinoshita, M. and Takiguchi, K. (2009). Septin-mediated uniform bracing
871 of phospholipid membranes. Curr. Biol. *2*, 140-145.

872 Tooley, A. J., Gilden, J., Jacobelli, J., Beemiller, P., Trimble, W. S., Kinoshita, M. and Krummel,
873 M. F. (2009). Amoeboid T lymphocytes require the septin cytoskeleton for cortical integrity and
874 persistent motility. Nat. Cell Biol. *1*, 17-26.

875 Vinayak, S., Pawlowic, M. C., Sateriale, A., Brooks, C. F., Studstill, C. J., Bar-Peled, Y.,
876 Cipriano, M. J. and Striepen, B. (2015). Genetic modification of the diarrhoeal pathogen
877 *Cryptosporidium parvum*. Nature *7561*, 477-480.

878 Wang, M. and Casey, P. J. (2016). Protein prenylation: unique fats make their mark on biology.
879 Nat. Rev. Mol. Cell Biol. *2*, 110-122.

880 Wilson, K. S., Gonzalez, O., Dutcher, S. K. and Bayly, P. V. (2015). Dynein-deficient flagella
881 respond to increased viscosity with contrasting changes in power and recovery strokes.
882 Cytoskeleton (Hoboken) *9*, 477-490.

883 Woznica, A., Cantley, A. M., Beemelmanns, C., Freinkman, E., Clardy, J. and King, N. (2016).
884 Bacterial lipids activate, synergize, and inhibit a developmental switch in choanoflagellates.
885 Proc. Natl. Acad. Sci. U. S. A. *28*, 7894-7899.

886 Woznica, A., Gerdt, J. P., Hulett, R. E., Clardy, J. and King, N. (2017). Mating in the Closest
887 Living Relatives of Animals Is Induced by a Bacterial Chondroitinase. Cell *6*, 1183.e11.

888 Yang, T. T., Cheng, L. and Kain, S. R. (1996). Optimized codon usage and chromophore
889 mutations provide enhanced sensitivity with the green fluorescent protein. Nucleic Acids Res.
890 *22*, 4592-4593.

891 Young, S. L., Diolaiti, D., Conacci-Sorrell, M., Ruiz-Trillo, I., Eisenman, R. N. and King, N.
892 (2011). Premetazoan ancestry of the Myc-Max network. Mol. Biol. Evol. *10*, 2961-2971.

893 **FIGURE LEGENDS**

894

895 **Figure 1: Introduction to *Salpingoeca rosetta*, an experimentally-tractable model**
896 **choanoflagellate**

897 **(A)** *S. rosetta* and other choanoflagellates (abbreviated as 'choano') are the closest living
898 relatives of animals. **(B, C)** *S. rosetta* has a complex life history that includes single cells **(B)** and
899 multicellular rosettes **(C)**. Immunofluorescence in fixed, permeabilized *S. rosetta* single cells **(B)**
900 highlights the diagnostic cellular architecture of choanoflagellates, including a single apical
901 flagellum (f) made of microtubules (white) surrounded by a collar (co) filled with F-actin (red) of
902 microvilli. Staining for tubulin also illuminates cortical microtubules (cm) that run in parallel
903 tracks along the cell periphery from the apical to the basal poles of each cell. DNA staining
904 (blue) highlights the choanoflagellate nucleus (n) and the nucleoids of bacterial prey (b) present
905 in choanoflagellate cultures. **(C)** In multicellular rosettes (stained as in panel **B**), the basal poles
906 of cells are oriented toward the interior of the rosette and the apical flagella point outward.

907

908 **Figure 2: A robust procedure for transfecting *S. rosetta***

909 **(A)** A summary of the step-wise procedure to transfect *S. rosetta* with DNA plasmids. To
910 prepare *S. rosetta* for transfection, cells were harvested at mid-log phase and then washed to
911 remove bacteria (depicted as grey ovals). *S. rosetta* cells (depicted with an apical collar,
912 flagellum, and nucleus; n) were primed for nucleofection (step 1) through washing with a buffer
913 that degrades extracellular material. A DNA plasmid encoding a highly sensitive luciferase,
914 nanoluc, or a fluorescent protein was then transfected into the nucleus with a nucleofector (step
915 2). Immediately after transfection, the cells rested in a buffer that promotes membrane closure
916 (step 3). Finally, the cells were transferred into 1x High Nutrient Media prepared with AK
917 seawater for two days (step 4) before we assayed the expression of nanoluc or fluorescent
918 proteins from the transfected DNA. **(B)** Non-coding DNA sequences flanking the coding
919 sequences for *S. rosetta elongation factor L* (pEFL), *α-tubulin* (pTub), *β-actin* (pAct), and
920 *histone H3* (pH3) genes drive the expression of a codon-optimized *nanoluc* reporter gene. 2.5
921 *μ*g of pEFL-*nanoluc,* pTub-*nanoluc,* pAct-*nanoluc*, and pH3-*nanoluc* reporter plasmids were
922 each transfected into *S. rosetta* and the cells were subsequently assayed for luciferase
923 expression. Each reporter produced a luminescence signal that was at least three orders of
924 magnitude greater than the detection limit (dotted line) and significantly greater (one-way

925 ANOVA, $p < 0.001$) than the background from a negative control, in which cells were
926 transfected with an empty pUC19 vector (None). See Materials and Methods for details on
927 replicates and statistical tests. **(C)** Systematically omitting each step of the transfection
928 procedure revealed critical steps for the delivery and expression of plasmid DNA in *S. rosetta*
929 cells. As a baseline for comparison, cells with 2.5 μg of pH3-*nanoluc* reporter (row b) produced
930 a luciferase signal that was three orders of magnitude greater than the background detected
931 from cells transfected without the reporter plasmid (row a). Omitting the priming step by
932 incubating cells in artificial seawater instead of priming buffer (row c), decreased luciferase
933 signal by over two orders of magnitude. Nucleofection without carrier DNA (row d) or the
934 application of the CM156 electrical pulse (row e) resulted in a complete loss of luciferase signal,
935 indicating that both were essential for successful transfection. Directly transferring cells to sea
936 water after nucleofection instead of a buffer that promotes membrane resealing during the rest
937 step (row f) decreased the luciferase signal almost ten-fold. Finally, despite the fact that most
938 prey bacteria were washed out prior to nucleofection, addition of fresh prey bacteria did not
939 appear to be necessary. Supplementing transfected cells with fresh prey bacteria at the start of
940 the recovery step had seemingly little effect on transfection success (row g), probably due to the
941 persistence of a small number of live bacteria throughout the nucleofection procedure. **(D and**
942 **E)** Fluorescent reporters mark transfected cells. Live cells transfected with a pAct-m*Wasabi*
943 reporter construct could be observed by fluorescence microscopy **(D)** and quantified by flow
944 cytometry **(E)**. Untransfected cells were used to draw a gate that includes 99.99% of cells, or
945 four-standard deviations above the mean fluorescence value (left). The same gate was applied
946 to a population of transfected cells (right) to categorize the mWasabi- population. Cells with
947 higher values of green fluorescence that laid outside of the mWasabi- gate are categorized as
948 mWasabi+. The efficiency of transformation, as quantified by three independent flow cytometry
949 experiments, was ~1% in a population of 1 million cells.
950
951 **Figure 3: Fluorescent markers illuminate the cell biology of *S. rosetta* in live cells**
952 Fluorescent subcellular markers expressed from reporter plasmids in live *S. rosetta* cells were
953 constructed by fusing *mCherry* in frame to genes encoding localization peptides and proteins
954 (Datasets S1 and S3). Twenty-four hours after co-transfecting cells with 5 μg of a plasmid
955 encoding a subcellular marker fused to the mCherry protein and 5 μg of a plasmid encoding
956 untagged mTFP1 that served as a whole cell marker, live cells were visualized by
957 superresolution microscopy with a Zeiss LSM 880 Airyscan. The variation in localization of the

958 whole cell mTFP1 marker stems from cell-to-cell differences in the number and localization of
959 vacuoles, which exclude mTFP1. In panels **A** - **I**, the cells are oriented with the apical flagellum
960 at the top and the nucleus, when included in the plane of focus (**A'' - F'')**, is indicated with a
961 dotted white line. **(A)** Without localization signals (None), fluorescent proteins (mCherry, **A'**, and
962 mTFP1, **A''**) were distributed throughout the cell with a slight enrichment in the nucleus and
963 complete exclusion from other membrane bound compartments. **(B and C)** A fusion of mCherry
964 to the carboxy terminus of Histone H3 **(B')** or the amino terminus of a simian virus 40 nuclear
965 localization signal **(**NLS; **C')** was confined to the nucleus, whereas mCherry fused to the
966 carboxy terminus of elongation factor L **(**EFL; **D)** was excluded from the nucleus and restricted
967 to the cytosol. **(E)** The endoplasmic reticulum (ER) was highlighted by fusing the signal
968 sequence from Rosetteless (PTSG_03555) and an ER retention sequence (HDEL from
969 PTSG_07223) to the amino and carboxy termini of mCherry, respectively. **(F)** The mitochondrial
970 network was highlighted by fusing a targeting sequence from *S. cerevisiae* CoxIV to the amino
971 terminus of mCherry. **(G)** A Lifeact peptide fused to the amino terminus of mCherry marked
972 filamentous actin (F-actin) that forms filipodia (arrowhead) and actin filaments in the cell body
973 that coalesce to form the collar (arrow). **(H)** Fusing mCherry to the amino terminus of α-Tubulin
974 highlighted parallel tracks of microtubules (arrowhead) that extended subcortically from the
975 apical pole to the basal pole of cells and microtubules that emerged from the apical pole of the
976 cell body to form the flagellum. The flagellum undulates rapidly in live cells and can be difficult to
977 image in total; in this cell the most distal tip of the flagellum is captured in the plane of focus
978 (arrow). **(I)** A plasma membrane marker constructed by fusing a geranyl-geranylation sequence
979 (PTSG_00306) to the carboxy terminus of mCherry outlined the entire cell shape, including the
980 collar, flagellum, and cell body. The membrane marker also weakly highlighted the Golgi
981 (arrowhead). The food vacuole (asterisk) was often visualized due to autofluorescence from
982 ingested bacteria or through accumulation of the fluorescent markers in the food vacuole,
983 perhaps through autophagy. **(J - L)** Orthogonal views along the xy and xz axes from confocal
984 micrographs showed fine details of cell architecture that were highlighted by transfecting cells
985 with F-actin, microtubule, and plasma membrane markers fused to mCherry (magenta). In xz
986 views, each cell is oriented with the flagellum facing toward the top of the micrograph; the
987 flagella appeared shorter and blurred because of the sigmoidal shape of the flagellar beat.
988 Lifeact **(J)** and the plasma membrane **(L)** markers fused to mCherry showed the microvilli
989 (arrowheads). **(K)** The α-tubulin-mCherry showed the subcortical tracks of microtubules at the
990 cell periphery (arrowhead) and the microtubule organizing center (arrow).

991

992 **Figure 4: Septins assemble at the basal pole of *S. rosetta* cells**

993 **(A)** *Sr*Septin2 has a prototypical protein domain architecture of septins, with an amino-terminal
994 Septin G-domain that mediates filament formation and a carboxy terminal coiled-coil domain
995 that mediates higher order assemblies of septin filaments. To investigate the localization of
996 *Sr*Septin2, we engineered fusions with mTFP1 at the amino terminus and created a truncation
997 of the coiled-coil domain (ΔCC). **(B)** A mTFP1-*Sr*Septin2 fusion protein localized to the basal
998 pole of unicellular cells (**B'**, arrowhead). Co-transfecting cells with mTFP1-*Sr*Septin2 and a
999 plasma membrane marker revealed *Sr*Septin2 distributed throughout the cytosol and enriched
1000 at the basal pole in confocal slices through the center of the cell. **(C)** mTFP1-*Sr*Septin6 mirrored
1001 the enrichment of mTFP1-*Sr*Septin2 at the basal pole (**C'**, arrowhead). The overlapping
1002 localization of *Sr*Septin2 and *Sr*Septin6 was compatible with these proteins forming heteromeric
1003 filaments with each other and other septin paralogs. **(D)** Consistent with the coiled-coil domain
1004 mediating the localization of septins through the formation of higher-order structures,
1005 *Sr*Septin2ΔCC localized throughout the cytoplasm, with no visible enrichment at the basal pole.
1006 Surprisingly, the deletion also caused ectopic filaments (**D'**; arrowheads) to form around
1007 membrane-bound vesicles that were, based on their size and position in the cell, presumably
1008 food vacuoles. **(E)** In rosettes, mTFP1-*Sr*Septin2 localized to points of cell-cell contact
1009 corresponding to the basal poles of cells (**E'**; arrowhead). **(F)** As in single cells, mTFP1-
1010 *Sr*Septin2ΔCC in rosettes was distributed throughout the cytosol and formed ectopic filaments
1011 (**F'**; arrowheads) around vacuoles. In panels **E** and **F**, *S. rosetta* single cells were transfected as
1012 in panels **B** and **C**, immediately induced to develop into rosettes (Woznica *et al.*, 2016), and
1013 imaged the next day. **(G)** *Sr*Septin2 intercalated between microtubules at the basal pole of the
1014 cell. Co-transfecting cells with mTFP1-*Sr*Septin2 and the α-tubulin marker showed *Sr*Septin2
1015 filaments intercalated between microtubules at the basal pole in confocal slices that capture the
1016 cell cortex to easily visualize microtubule tracks. (**G'**, **G''**, **G'''**; box). **G''''** shows a 4x
1017 magnification of the basal pole of a representative cell (boxed region from **G'**, **G''**, **G'''**). In
1018 panels B-F, autofluorescence from ingested bacteria or through accumulation of the fluorescent
1019 markers highlights the food vacuole (asterisk).

Figure 1

Introduction to *Salpingoeca rosetta*, an experimentally-tractable model choanoflagellate

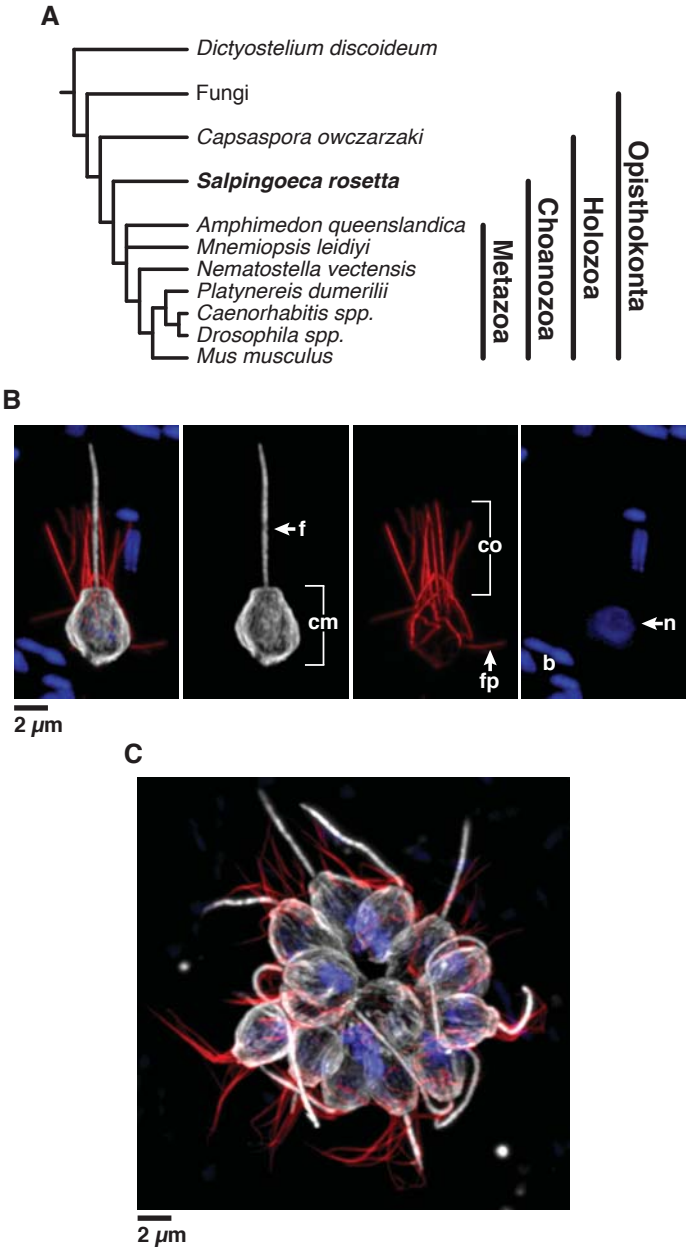

Figure 2

A robust procedure for transfecting *S. rosetta*

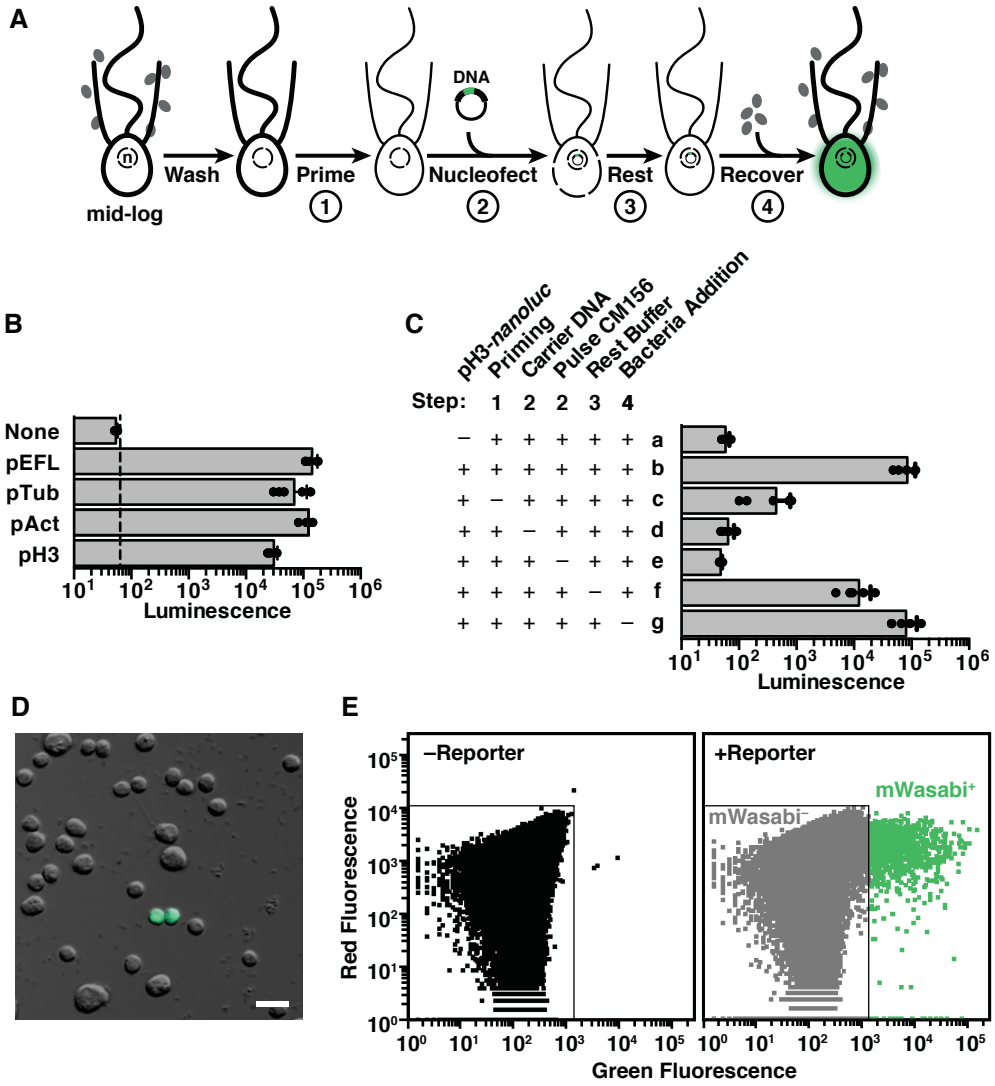

Figure 3

Fluorescent markers illuminate the cell biology of *S. rosetta* in live cells

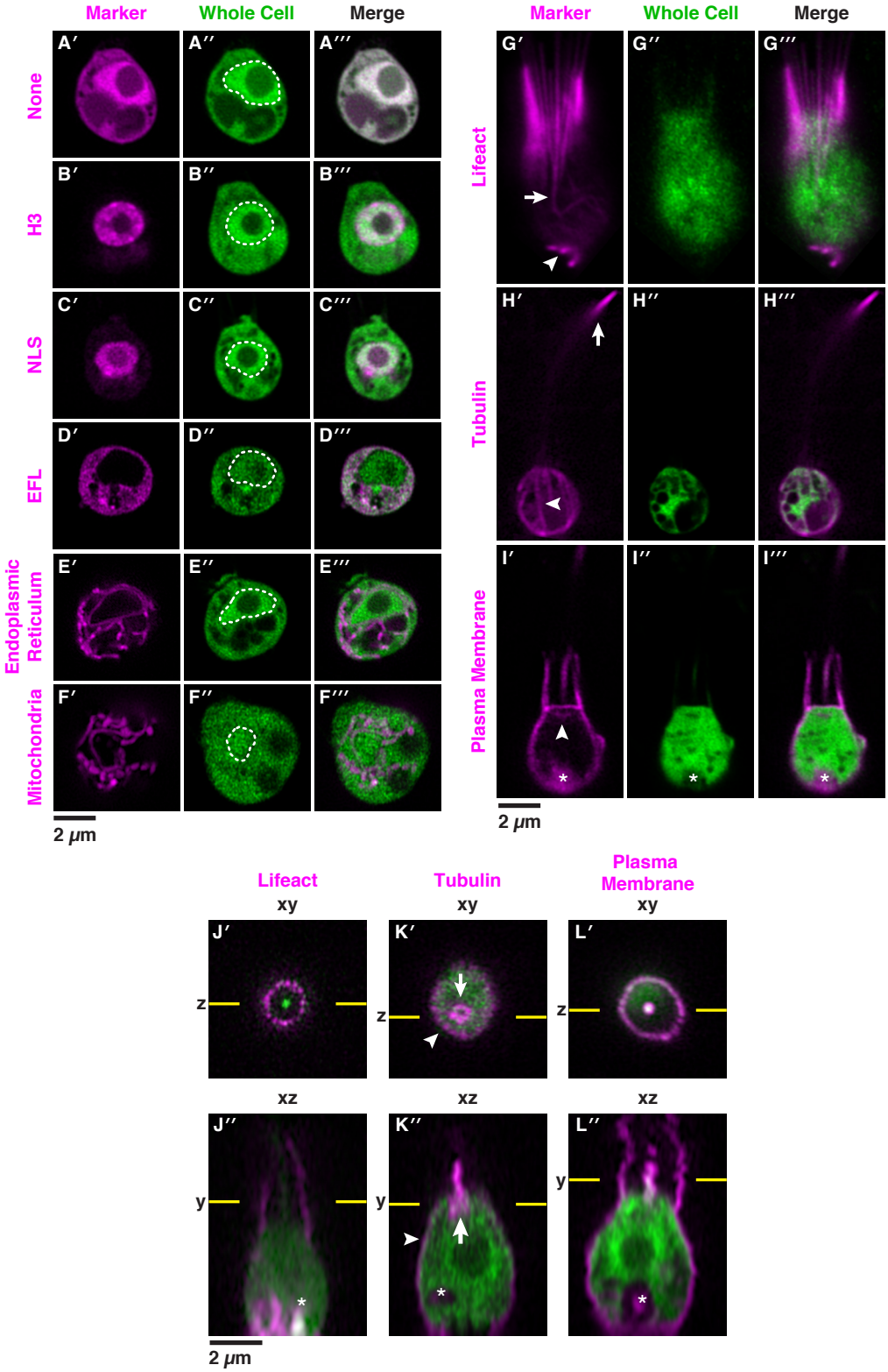

Figure 4
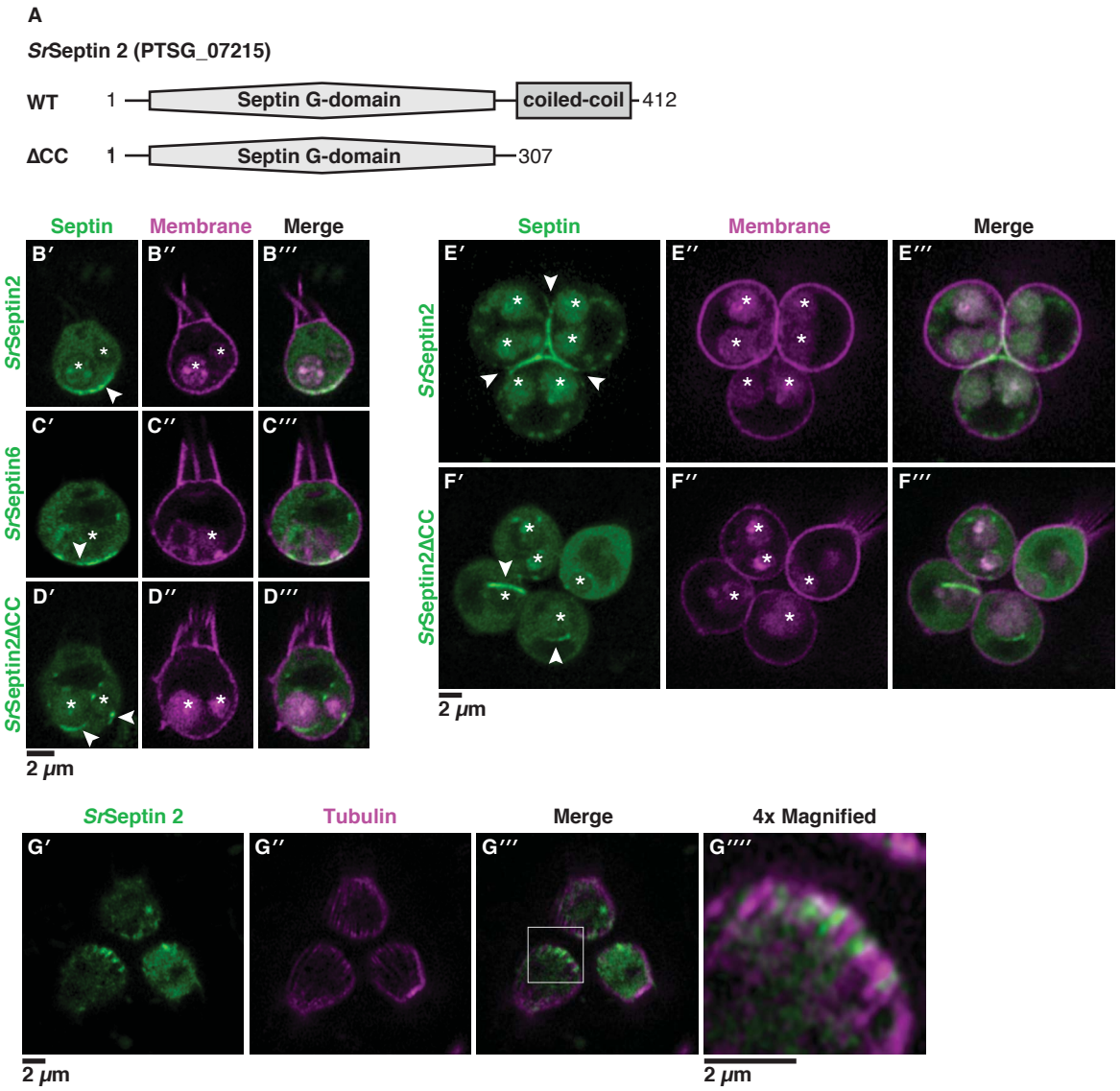
Septins assemble at the basal pole of *S. rosetta* cells